

Quantum-inspired canonical correlation analysis for exponentially large dimensional data

Naoko Koide-Majima

Kyoto, Japan

nkmajima@gmail.com

Kei Majima

Kyoto, Japan

majimajimajimajima@gmail.com

Abstract

Canonical correlation analysis (CCA) is a technique to find statistical dependencies between a pair of multivariate data. However, its application to high dimensional data is limited due to the resulting time complexity. While the conventional CCA algorithm requires polynomial time, we have developed an algorithm that approximates CCA with computational time proportional to the logarithm of the input dimensionality using quantum-inspired computation. The computational efficiency and approximation performance of the proposed quantum-inspired CCA (qiCCA) algorithm are experimentally demonstrated. Furthermore, the fast computation of qiCCA allows us to directly apply CCA even after nonlinearly mapping raw input data into very high dimensional spaces. Experiments performed using a benchmark dataset demonstrated that, by mapping the raw input data into the high dimensional spaces with second-order monomials, the proposed qiCCA extracted more correlations than linear CCA and was comparable to deep CCA and kernel CCA. These results suggest that qiCCA is considerably useful and quantum-inspired computation has the potential to unlock a new field in which exponentially large dimensional data can be analyzed.

Introduction

Canonical correlation analysis (CCA) is a technique to find statistical dependencies between a pair of multivariate data (1). While CCA and its variants have become a key tool in various fields, such as neuroscience and bioinformatics (2–16), its application to high dimensional data (*i.e.*, data with a large number input features) is limited due to its expensive time complexity.

In this study, we present an algorithm that approximates CCA with computational time proportional to the logarithm of the input dimensionality. The proposed algorithm is based on quantum-inspired algorithms, which are recently developed randomized algorithms for linear algebra computations (17–21). In this paper, we first explain our proposed quantum-inspired CCA (qiCCA) algorithm and then experimentally demonstrate its computational efficiency and approximation performance.

Furthermore, the fast computation of our algorithm enables us to directly apply CCA even after nonlinearly mapping raw input data into high dimensional spaces. Previous studies have shown that kernel CCA (22–26) and deep CCA (27, 28) can extract more correlations than linear CCA by nonlinearly mapping raw input data into high dimensional spaces. While kernel CCA and deep CCA utilize the kernel trick and neural networks for their nonlinear transformation, mapping raw input data using a set of multivariate basis functions, such as polynomial or Fourier basis functions, seems a simple and straightforward approach; however, after nonlinear mapping, the dimensionality increases exponentially against the dimensionality of the raw input data. This makes it computationally infeasible to apply the conventional CCA. In an experiment with a benchmark dataset, we mapped the raw input data into high dimensional spaces by taking the products of the input features for all possible feature pairs and applied qiCCA on the resultant high dimensional data. The results demonstrated that qiCCA extracted more correlations than linear CCA and was comparable to kernel and deep CCA. This suggests that the combination of qiCCA and nonlinear mapping using a large number of basis functions can provide an alternative way to reveal nonlinear correlations.

Algorithm

This section is organized as follows. First, we explain the mathematical notations. Then, we introduce the conventional CCA algorithm in which singular value decomposition (SVD) is used as a subroutine. In the following subsections, we explain quantum-inspired SVD (qiSVD) and the data structure that allows us to perform qiSVD in logarithmic time. Finally, we explain the qiCCA algorithm. Note that a Python implementation of qiCCA is available at our GitHub repository¹.

Notations

We denote the set of $I \times J$ real matrices by $\mathbb{R}^{I \times J}$. For a matrix $\mathbf{A} \in \mathbb{R}^{I \times J}$, we denote the (i, j) -entry by $\mathbf{A}(i, j)$, the i -th row by $\mathbf{A}(i, :)$, and the j -th column by $\mathbf{A}(:, j)$. The $I \times K$ matrix that consists of the first K columns of \mathbf{A} is denoted $\mathbf{A}(:, 1:K)$, and the $K \times J$ matrix that consists of the first K rows of \mathbf{A} is denoted $\mathbf{A}(1:K, :)$. The transpose, inverse, and Frobenius norm of \mathbf{A} are denoted \mathbf{A}^T , \mathbf{A}^{-1} , and $\|\mathbf{A}\|_F$, respectively. Similarly, we denote the set of N -dimensional real column vectors by \mathbb{R}^N . For a vector $\mathbf{v} \in \mathbb{R}^N$, we denote its n -th element by $\mathbf{v}(n)$. The transpose and Euclidean norm of \mathbf{v} are denoted \mathbf{v}^T and $\|\mathbf{v}\|$, respectively.

Canonical correlation analysis

We introduce the CCA algorithm in which SVD is used as a subroutine. We assume a pair of data matrices, $\mathbf{X} \in \mathbb{R}^{N \times D_1}$ and $\mathbf{Y} \in \mathbb{R}^{N \times D_2}$, where N is the number of samples and D_1 and D_2 indicate the numbers of input dimensions (*i.e.*, input features). The first K pairs of the canonical variates and their linear weights can be obtained by the following operations.

1. Perform SVD on \mathbf{X} and \mathbf{Y} . Denote the results as

$$\mathbf{X} = \mathbf{U}_1 \mathbf{\Sigma}_1 \mathbf{V}_1^T, \mathbf{Y} = \mathbf{U}_2 \mathbf{\Sigma}_2 \mathbf{V}_2^T.$$

2. Compute $\mathbf{U}_1^T \mathbf{U}_2$ and perform SVD on the result. Denote the results by

$$\mathbf{U}_1^T \mathbf{U}_2 = \mathbf{U}_3 \mathbf{\Sigma}_3 \mathbf{V}_3^T.$$

3. Compute the first K pairs of the canonical variates as

$$\mathbf{C}_X = \mathbf{U}_1 \mathbf{U}_3(:, 1:K), \mathbf{C}_Y = \mathbf{U}_2 \mathbf{V}_3(:, 1:K).$$

4. Compute the linear weights for the above canonical variates as

¹ <https://github.com/nkmjm/qiML>

$$\mathbf{W}_X = \mathbf{V}_1 \boldsymbol{\Sigma}_1^{-1} \mathbf{U}_3(:, 1:K), \mathbf{W}_Y = \mathbf{V}_2 \boldsymbol{\Sigma}_2^{-1} \mathbf{V}_3(:, 1:K).$$

In last subsection, the qiCCA algorithm is obtained by replacing the SVD in step 1 of the above algorithm with qiSVD.

Quantum-inspired singular value decomposition

We explain qiSVD based on a previous study (17). For a given matrix $\mathbf{X} \in \mathbb{R}^{I \times J}$, the standard SVD algorithm provides a low-rank (K -rank) approximation of the given matrix as $\mathbf{U}\boldsymbol{\Sigma}\mathbf{V}^T$. Here, $\boldsymbol{\Sigma} \in \mathbb{R}^{K \times K}$ is the diagonal matrix whose (k, k) -entry is the k -th largest singular value, and $\mathbf{U} \in \mathbb{R}^{I \times K}$ and $\mathbf{V} \in \mathbb{R}^{J \times K}$ are the matrices whose columns are the left- and right-singular vectors corresponding to the top K singular values, respectively. qiSVD computes a “description” of \mathbf{V} (17, 29). A description of \mathbf{V} is the set of a matrix $\mathbf{S} \in \mathbb{R}^{P \times J}$ and vectors $\mathbf{u}_k \in \mathbb{R}^P (k = 1, 2, \dots, K)$ that approximate $\mathbf{V}(:, k)$ by $\mathbf{S}^T \mathbf{u}_k$ where P is a parameter that controls the trade-off between computational time and approximation performance. Once a description of \mathbf{V} is obtained, we can access any entry of the approximation of \mathbf{V} in constant time regardless of the size of the input matrix. The qiSVD procedure for a given matrix $\mathbf{X} \in \mathbb{R}^{I \times J}$ is as follows.

1. Sample from the categorical distribution that takes $i \in \{1, 2, \dots, I\}$ with probability

$$f_i = \frac{\|\mathbf{X}(i, :)\|^2}{\|\mathbf{X}\|_F^2}.$$

Repeat this P times and denote the results by i_1, i_2, \dots, i_P .

2. Sample from the categorical distribution that takes $j \in \{1, 2, \dots, J\}$ with probability

$$g_j = \frac{1}{P} \sum_{p=1}^P \frac{\mathbf{X}(i_p, j)^2}{\|\mathbf{X}(i_p, :)\|^2}.$$

Repeat this P times and denote the results by j_1, j_2, \dots, j_P .

3. Let \mathbf{W} be the $P \times P$ matrix whose (p, q) -entry is

$$\frac{\mathbf{X}(i_p, j_q)}{P \sqrt{f_{i_p} g_{j_q}}},$$

and perform SVD on \mathbf{W} . Denote the top K singular values and the corresponding left singular vectors by σ_k and $\mathbf{u}'_k \in \mathbb{R}^P (k = 1, 2, \dots, K)$.

4. Let \mathbf{S} be the $P \times J$ matrix whose p -th row is $\mathbf{X}(i_p, :)$, and let $\hat{\mathbf{u}}_k \in \mathbb{R}^P$ be the vector

whose p -th element is $\mathbf{u}'_k(p)/(\sigma_k\sqrt{pf_p})$.

5. Orthonormalize $\{\mathbf{S}^T\hat{\mathbf{u}}_k\}_{k=1}^K$ by applying the Gram–Schmidt process, and obtain a new set of vectors $\{\mathbf{u}_k\}_{k=1}^K$ such that $\{\mathbf{S}^T\mathbf{u}_k\}_{k=1}^K$ is an orthonormal set (see **Appendix** for a complete explanation).
6. Output \mathbf{S} and \mathbf{u}_k ($k = 1, 2, \dots, K$) as a description of the right singular vectors of \mathbf{X} .

The above algorithm can be performed in $O(\log IJ)$ time when we use the input data structure explained in the next subsection. In steps 1 and 2 of the above algorithm, we perform random sampling, which can be interpreted as analogous to quantum computation. In quantum computation, a superposition of states is represented by a linear combination of the corresponding vectors, and we can sample each state with the probability proportional to its squared coefficient in constant time regardless of the dimensionality of the vectors. Utilizing this, quantum computation provides quantum algorithms to compute several basic algebraic calculations (*e.g.*, taking the inner product between two vectors) faster than their classical counterparts and leads to several quantum machine learning algorithms (30–33).

The original qiSVD algorithm proposed by Tang (2019) does not include step 5 of the above algorithm and does not provide an orthonormal set of vectors. The orthonormalization step was introduced to obtain an orthonormal set of vectors that approximates singular vectors used in CCA. The full explanation of this step is given in the appendix. The approximation performance of this algorithm has been investigated analytically in previous studies (17, 29). We also demonstrate the approximation performance of qiSVD numerically in the results section of this paper.

Data structure

Here, we introduce the data structure that we use for qiSVD and qiCCA. By using a binary search tree with N leaves for an N -dimensional vector $\mathbf{x} \in \mathbb{R}^N$ (Figure 1A), we can sample from the categorical distribution that takes n ($n = 1, 2, \dots, N$) with probability $\mathbf{x}(n)^2/\|\mathbf{x}\|^2$ in $O(\log N)$ time, which is faster than naïve sampling algorithms without binary search trees, such as that adopted in SciPy (Figure 1B). To perform the sampling operations required in step 1 of qiSVD for an input matrix $\mathbf{X} \in \mathbb{R}^{I \times J}$, we prepared a binary search tree with I leaves. This allows us to perform the required samplings in $O(\log I)$ time. To perform the sampling operations required in step 2, we prepared I binary search trees with J leaves that

stored the individual rows of the matrix. In step 2, we uniformly and randomly selected an index from $\{i_1, i_2, \dots, i_p\}$ and then sampled from the categorical distribution using the binary search tree corresponding to the row specified by the selected index. This is equivalent to the sampling required in step 2 of qiSVD, and this can be done in $O(\log J)$ time. A total of $(I + 1)$ binary search trees were used to store the matrix. Variants of this binary tree data structure are described in the literature (17, 34).

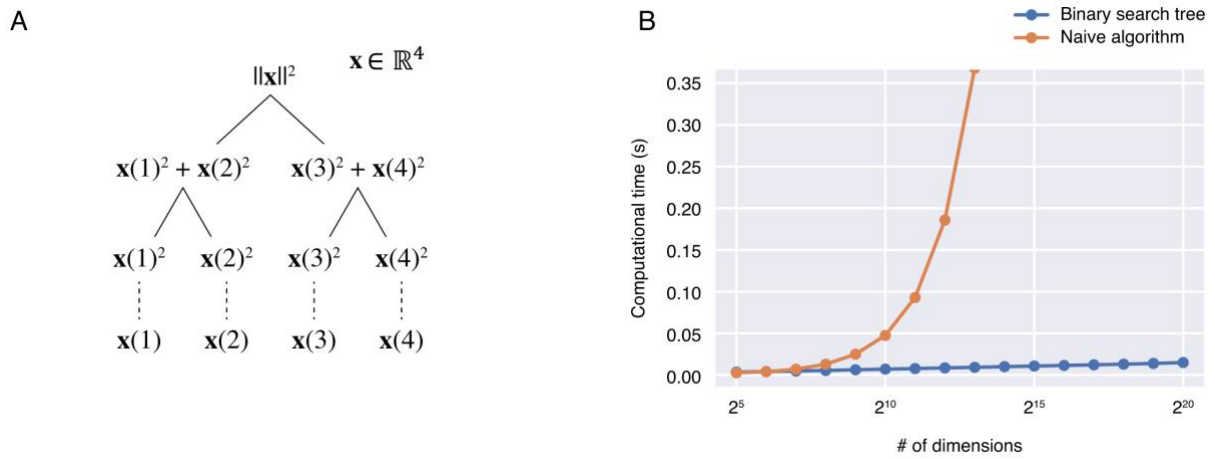


Figure 1. Binary tree data structure and sampling. (A) Binary tree data structure. To store an N -dimensional vector, a binary search tree with N leaves is used. This allows us to sample from the categorical distribution that takes n ($n = 1, 2, \dots, N$) with probability proportional to the square of the n -th element of the vector. (B) Computational time. The mean computational time to sample from the categorical distribution across 10 repetitions is shown as a function of the number of the dimensions. The algorithm using the binary tree data structure is compared to a naïve algorithm that takes time proportional to the number of the dimensions.

Quantum-inspired canonical correlation analysis

For qiCCA, we assume a pair of input matrices $\mathbf{X} \in \mathbb{R}^{N \times D_1}$ and $\mathbf{Y} \in \mathbb{R}^{N \times D_2}$ where N is the number of samples and D_1 and D_2 indicate the number of input dimensions. \mathbf{X}^T and \mathbf{Y}^T are stored using the binary tree data structure explained in the previous subsection. In the qiCCA algorithm, a pair of descriptions that approximate the first K canonical variates and a pair of descriptions that approximate the linear weight matrices for the canonical variates are computed as follows.

1. Perform qiSVD on \mathbf{X}^T . Denote the resultant description of the left singular vectors of \mathbf{X} by $\mathbf{S}^{(1)}$ and $\{\mathbf{u}_l^{(1)}\}_{l=1}^L$. Denote the sampled indices in the first step of qiSVD by

$$\{i_1^{(1)}, i_2^{(1)}, \dots, i_{P_1}^{(1)}\}.$$

2. Perform qiSVD on \mathbf{Y}^T . Denote the resultant description of the left singular vectors of \mathbf{Y} by $\mathbf{S}^{(2)}$ and $\{\mathbf{u}_m^{(2)}\}_{m=1}^M$. Denote the sampled indices in the first step of qiSVD by

$$\{i_1^{(2)}, i_2^{(2)}, \dots, i_{P_2}^{(2)}\}.$$

3. Compute $(\mathbf{u}_1^{(1)}, \mathbf{u}_2^{(1)}, \dots, \mathbf{u}_L^{(1)})^T \mathbf{S}^{(1)} \mathbf{S}^{(2)T} (\mathbf{u}_1^{(2)}, \mathbf{u}_2^{(2)}, \dots, \mathbf{u}_M^{(2)})$ and perform SVD on it. Denote the results by $\mathbf{U} \mathbf{\Sigma} \mathbf{V}^T$.

4. Compute $(\mathbf{u}_1^{(1)}, \mathbf{u}_2^{(1)}, \dots, \mathbf{u}_L^{(1)}) \mathbf{U}(:, 1:K)$ and $(\mathbf{u}_1^{(2)}, \mathbf{u}_2^{(2)}, \dots, \mathbf{u}_M^{(2)}) \mathbf{V}(:, 1:K)$. Denote the results by

$$(\mathbf{w}_1^{(1)}, \mathbf{w}_2^{(1)}, \dots, \mathbf{w}_K^{(1)}) = (\mathbf{u}_1^{(1)}, \mathbf{u}_2^{(1)}, \dots, \mathbf{u}_L^{(1)}) \mathbf{U}(:, 1:K)$$

and

$$(\mathbf{w}_1^{(2)}, \mathbf{w}_2^{(2)}, \dots, \mathbf{w}_K^{(2)}) = (\mathbf{u}_1^{(2)}, \mathbf{u}_2^{(2)}, \dots, \mathbf{u}_M^{(2)}) \mathbf{V}(:, 1:K).$$

5. Output $\mathbf{S}^{(1)}$ and $\{\mathbf{w}_k^{(1)}\}_{k=1}^K$ as a description of the first K canonical variates from \mathbf{X} , and output $\mathbf{S}^{(2)}$ and $\{\mathbf{w}_k^{(2)}\}_{k=1}^K$ as a description of the first K canonical variates from \mathbf{Y} .

6. Prepare the $P_1 \times D_1$ binary matrix $\mathbf{A}^{(1)}$ whose (p, d) -entry is 1 if $i_p^{(1)} = d$ and 0

otherwise. Prepare the $P_2 \times D_2$ binary matrix $\mathbf{A}^{(2)}$ whose (p, d) -entry is 1 if $i_p^{(2)} = d$ and 0 otherwise.

7. Output $\mathbf{A}^{(1)}$ and $\{\mathbf{w}_k^{(1)}\}_{k=1}^K$ as a description of the weight vectors to extract the canonical variates from \mathbf{X} . Output $\mathbf{A}^{(2)}$ and $\{\mathbf{w}_k^{(2)}\}_{k=1}^K$ as a description of the weight vectors to extract the canonical variates from \mathbf{Y} .

The results of the above algorithm are equivalent to those of CCA when the input matrices are low-rank and qiSVD provides the exact left singular vectors. Thus, the qiCCA algorithm can be considered to approximate CCA. Estimating the approximation performance of this algorithm analytically is difficult; thus, we evaluate it numerically in the results section. In the subsequent numerical experiments, we set $L = M = 1000$, and P_1 and P_2 were set to 20% larger than L and M .

When we focus on the relationship between the computational cost of the algorithm and the input dimensionalities, the above algorithm takes $O(\log(D_1 D_2))$ time. In addition, we can efficiently obtain the canonical variates for new data using the weight vectors derived from the above algorithm. To obtain the k -th canonical variates for a new data matrix $\mathbf{X}_{\text{new}} \in \mathbb{R}^{N_{\text{new}} \times D_1}$, we calculate $\mathbf{X}_{\text{new}} \mathbf{A}^{(1)\top} \mathbf{w}_k^{(1)}$. By utilizing the fact that $\mathbf{A}^{(1)}$ is a sparse matrix, we can compute each entry of $\mathbf{X}_{\text{new}} \mathbf{A}^{(1)\top} \mathbf{w}_k^{(1)}$ in constant time regardless of the input dimensionality (D_1). Furthermore, while we primarily emphasize computational efficiency with respect to input dimensionalities in this study, the computational time of the above algorithm with respect to the number of input samples (N) can be also reduced from $O(N)$ to $O(\log N)$ by a randomized algorithm. In step 3 of qiCCA, we compute

$(\mathbf{u}_1^{(1)}, \mathbf{u}_2^{(1)}, \dots, \mathbf{u}_L^{(1)})^\top \mathbf{S}^{(1)} \mathbf{S}^{(2)\top} (\mathbf{u}_1^{(2)}, \mathbf{u}_2^{(2)}, \dots, \mathbf{u}_M^{(2)})$, which requires computational time proportional to N . By using the randomized algorithm to compute the inner product (explained in the Appendix), each entry of $\mathbf{S}^{(1)} \mathbf{S}^{(2)\top}$ can be approximately computed in $O(\log N)$ time.

Results

First, we evaluated the computational time and approximation performance of qiSVD, and then evaluated the computational time and performance of qiCCA. We also experimentally demonstrated that the computational efficiency of qiCCA enables us to perform CCA even after nonlinearly mapping original input data into high dimensional spaces, which provides a way to extract more correlations than linear CCA. These analyses were all performed using virtual machines on Amazon Elastic Compute Cloud (EC2). The instance type p2.xlarge was used when we performed the computation with deep CCA, and r5.12xlarge was used for all other experiments.

We evaluated the computational time of qiSVD. In our numerical experiment, the input matrix $\mathbf{X} \in \mathbb{R}^{I \times J}$ was synthesized by $\mathbf{X} = \mathbf{Z}\mathbf{W}$ where \mathbf{Z} and \mathbf{W} are $(I \times 100)$ - and $(100 \times J)$ -matrices whose each entry was sampled from the standard normal distribution. J was set to a fixed number (10000). The computational time of the conventional SVD and qiSVD algorithms was measured while changing the number of rows of the input matrix (Figure 2A). The qiSVD algorithm is exponentially faster than the conventional SVD algorithm.

Next, we evaluated the approximation performance of qiSVD. Using the above input matrix, we computed $\|\mathbf{X} - \mathbf{X}\mathbf{V}\mathbf{V}^T\|_F^2 / \|\mathbf{X}\|_F^2$ where \mathbf{V} is the matrix that consists of the (exact or approximated) right singular vectors corresponding to the top k singular values. This value measures the difference between the input matrix and its low-rank approximation obtained by \mathbf{V} . We compared this value for conventional SVD and qiSVD while changing k (Figure 2B). qiSVD shows results similar to those of the conventional SVD, indicating that qiSVD can provide a set of vectors that span a subspace similar to the subspace spanned by the exact right singular vectors.

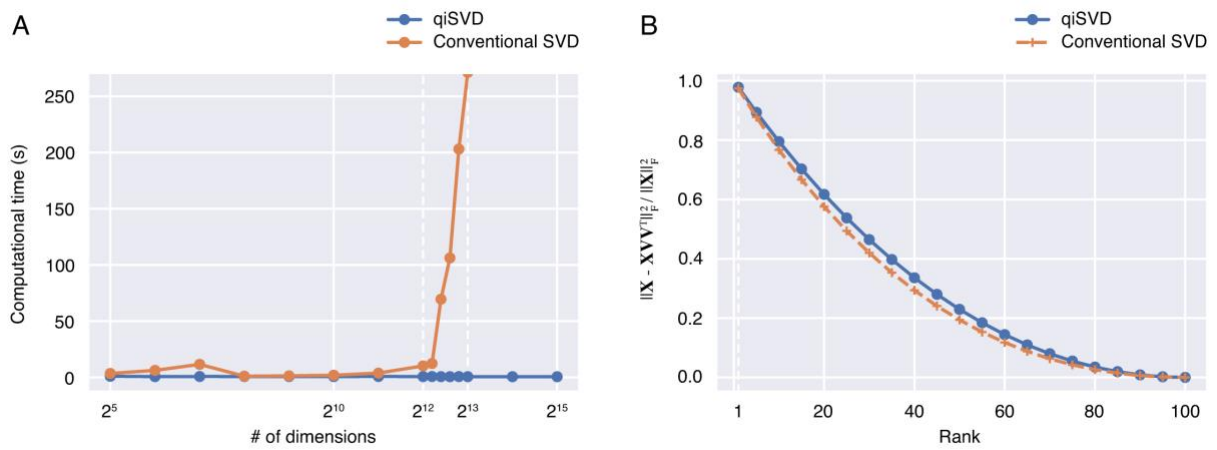


Figure 2. Computational time and approximation performance of qiSVD. (A)

Computational time. The mean computational time to perform SVD across 10 repetitions is shown as a function of the number of the rows of the input matrix. The qiSVD algorithm and the conventional SVD algorithm are compared. **(B)** Approximation performance. The mean error between the original input matrix and its low-rank approximation obtained by SVD across 10 repetitions is shown as a function of rank. The qiSVD algorithm and the conventional SVD algorithm are compared. The numbers of the columns and rows of the input matrix are set to 10000.

We then evaluated the computational time and performance of qiCCA. In a numerical experiment, we prepared a pair of input matrices $\mathbf{X} \in \mathbb{R}^{N \times D_1}$ and $\mathbf{Y} \in \mathbb{R}^{N \times D_2}$ by following the standard assumption of probabilistic CCA (35).

$$\mathbf{X} = \mathbf{Z}\mathbf{B}_1 + 0.5\mathbf{E}_1, \mathbf{Y} = \mathbf{Z}\mathbf{B}_2 + 0.5\mathbf{E}_2,$$

where $\mathbf{Z} \in \mathbb{R}^{N \times K}$, $\mathbf{B}_1 \in \mathbb{R}^{K \times D_1}$, $\mathbf{B}_2 \in \mathbb{R}^{K \times D_2}$, $\mathbf{E}_1 \in \mathbb{R}^{N \times D_1}$, and $\mathbf{E}_2 \in \mathbb{R}^{N \times D_2}$ are matrices whose each entry was sampled from the standard normal distribution. N and K were set to 10000 and 100. D_1 and D_2 were set to the same number and changed across $\{2^5, 2^6, \dots, 2^{15}\}$. We evaluated the computational time of qiCCA and CCA (Figure 3A). qiCCA showed an exponential speed-up over the conventional CCA. To evaluate the performance, following the procedure in previous studies (27, 28), we computed the canonical correlation for each pair of canonical variates and took the sum of them up to the first k canonical components (Figure 3B). qiCCA extracted almost the same degree of correlation as the conventional CCA.

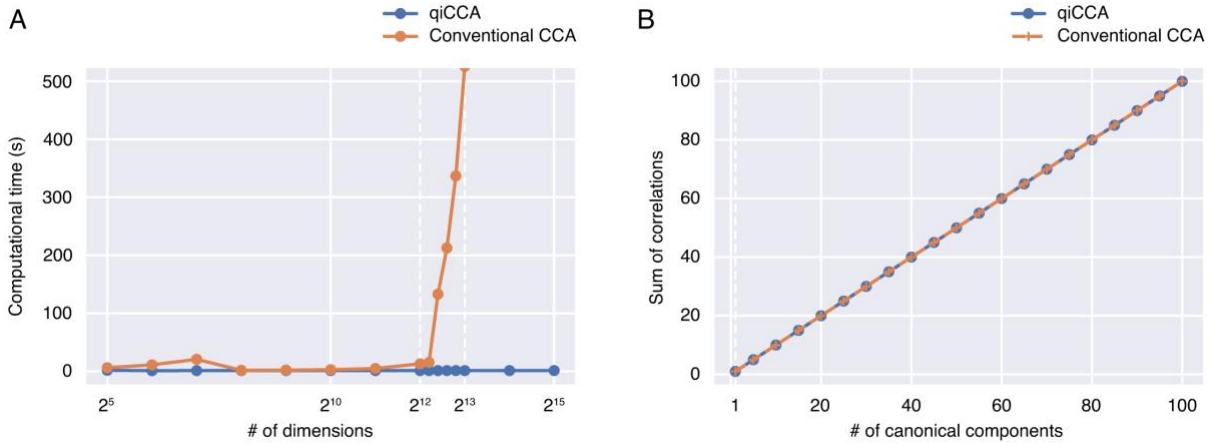


Figure 3. Computational time and approximation performance of qiCCA. (A)

Computational time. The mean computational time to perform CCA across 10 repetitions is shown as a function of the number of input dimensions (*i.e.*, input features). The qiCCA algorithm and the conventional CCA algorithm are compared. **(B)** Extractable correlations. The sum of the top k canonical correlations is shown as a function of k . The number of columns and rows of the input matrices are set to 10000. The qiCCA algorithm is compared to the conventional CCA.

Next, we demonstrate that the computational efficiency of qiCCA is helpful to extract more correlations by combining it with nonlinear mapping into high dimensional spaces. Previous studies have shown that kernel CCA (22–26) and deep CCA (27, 28) can extract more correlations than linear CCA by utilizing nonlinear mappings via the kernel trick and neural networks, respectively. As an alternative to the kernel trick or neural networks, just taking high order polynomials provides a simple and straightforward nonlinear transformation; however, the number of possible monomials increases exponentially when the number of input dimensions (*i.e.*, input features) increases. Although the kernel trick can treat such nonlinear transformations implicitly, the training of kernel CCA requires $O(N^3)$ time for N training samples and applying kernel CCA to data comprising several thousands of samples is difficult. The fast computation of qiCCA would be helpful when we want to apply CCA to such resultant high dimensional data. To illustrate this, we applied qiCCA after mapping the raw input data in each view (*i.e.*, each of \mathbf{X} and \mathbf{Y}) into high dimensional space using second-order monomials, and compared the extractable correlations with those obtained using kernel CCA and deep CCA.

For each of a pair of input matrices, we concatenated the raw input features and the products of the input features for all possible feature pairs and applied qiCCA. We refer to this method as “qiCCA + 2nd-order.” In this section, the method where qiCCA is applied only to the raw input features is referred to as “qiCCA + 1st-order.” We compared the extractable correlations between qiCCA + 1st-order, qiCCA + 2nd-order, kernel CCA, and deep CCA using the MNIST dataset (36). This MNIST dataset has been used as a benchmark dataset to test variants of CCA in several previous studies (27, 28). Following the procedure used in a previous study (27), the pixel values of the left and right 14 columns in 28 x 28 handwritten digit images were treated as a pair of input data. The number of raw input dimensions in each view is 392, and the number of input dimensions for qiCCA + 2nd-order is 77420, which is a huge number of dimensions that conventional CCA cannot handle even over more than two days of computational time in the same computational environment. Following the procedure used in the previous study (27), we fitted each CCA model using 50000 training samples, and evaluated generalization performance on 10000 test samples. For kernel CCA and deep CCA, the hyperparameters and architecture were optimized using the same procedure as the previous study (27).

The correlations extracted by each method is shown in Figure 4. qiCCA + 2nd-order extracted more correlations than qiCCA + 1st-order, and was comparable with kernel and deep CCA.

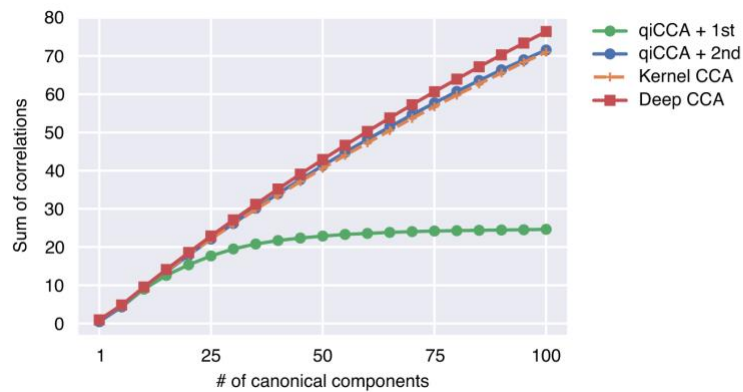


Figure 4. Extractable correlations on MNIST dataset. The sum of the top k canonical correlations is shown as a function of k . qiCCA + 1st-order, qiCCA + 2nd-order, kernel CCA, and deep CCA are compared.

Discussion

We developed qiCCA and numerically demonstrated its computational efficiency (Figure 3A) and performance (Figure 3B) compared to conventional CCA. We have also demonstrated that, by combining it with nonlinear mappings to high dimensional spaces, qiCCA extracted more correlations than linear CCA and was comparable to kernel and deep CCA on a benchmark dataset (Figure 4).

In an experiment with a benchmark dataset, we mapped the raw input data into high dimensional spaces by taking the second-order monomials. By using a complete set of basis functions, such as Fourier basis functions or monomials, we can approximate an arbitrary function as a linear combination of them, which enables us to extract nonlinear correlations by applying linear CCA. However, the number of monomials whose order is less than a given number or the number of Fourier basis functions whose frequency is less than a given value rapidly increases as the input dimensionality of the raw data increases, which makes it computationally infeasible to apply conventional CCA. The kernel trick can treat such nonlinear transformations implicitly. However, training kernel CCA takes $O(N^3)$ time for N training samples, and applying kernel CCA to a dataset that consists of several thousands of samples is difficult. The fast computation of qiCCA would be useful in situations where treatment of large amounts of data is required.

While we primarily emphasized the fact that the computational time of qiCCA is proportional to the logarithm of the number of input dimensions, the computational time is also proportional to the logarithm of the number of input samples (see the **Algorithm** section and **Appendix**). Training a machine learning model with a large number of samples is the most straightforward approach to prevent overfitting. However, most existing machine learning methods require exponentially large time when the number of training samples is increased exponentially, which limits the use of those methods when a large amount of data is involved. The computational efficiency of qiCCA and quantum-inspired computation would be helpful when training a model on a large number of training samples is required.

Taken together, our results suggest that qiCCA is considerably useful and quantum-inspired computation has the potential to unlock a new field in which exponentially large dimensional data can be analyzed.

Appendix

We explain the procedure for step 5 in the qiSVD algorithm. We follow the notations adopted in the algorithm section in the main text. Thus, we denote the input matrix by \mathbf{X} , the indices sampled in step 1 of the qiSVD algorithm by $\{i_1, i_2, \dots, i_p\}$, and the vectors obtained in step 4 of the qiSVD algorithm by $\{\hat{\mathbf{u}}_k\}_{k=1}^K$. The procedure of step 5 is as follows.

1. Compute the $P \times P$ matrix \mathbf{M} whose (p, q) -entry is $\mathbf{X}(i_p, :)\mathbf{X}(i_q, :)^T$.
2. Compute

$$\mathbf{u}_1 = \frac{\hat{\mathbf{u}}_1}{\sqrt{\hat{\mathbf{u}}_1^T \mathbf{M} \hat{\mathbf{u}}_1}},$$

and set k to 2.

3. Compute

$$\mathbf{v}_k = \hat{\mathbf{u}}_k - \sum_{l=1}^{k-1} (\hat{\mathbf{u}}_k^T \mathbf{M} \mathbf{u}_l) \mathbf{u}_l.$$

4. Compute

$$\mathbf{u}_k = \frac{\mathbf{v}_k}{\sqrt{\mathbf{v}_k^T \mathbf{M} \mathbf{v}_k}},$$

and set k to $(k + 1)$.

5. Repeat steps 3) and 4) until k reaches K .
6. Output $\{\mathbf{u}_k\}_{k=1}^K$.

In the same manner as the Gram–Schmidt process, $\{\mathbf{S}^T \mathbf{u}_k\}_{k=1}^K$ would be an orthonormal set where \mathbf{S} is the matrix whose p -th row is $\mathbf{X}(i_p, :)$.

The above algorithm takes constant time regardless of the number of the rows of the input matrix. Furthermore, although step 1 takes time proportional to the number of the columns of \mathbf{X} , optionally, the computational time for step 1 of this algorithm can be exponentially reduced by the following randomized algorithm. For a pair of N -dimensional vectors \mathbf{x} and \mathbf{y} , the inner product (\mathbf{x}, \mathbf{y}) can be approximately computed as follows.

1. Sample from the categorical distribution that takes $n \in \{1, 2, \dots, N\}$ with probability

$$h_n = \frac{\mathbf{x}(n)^2}{\|\mathbf{x}\|^2}$$

P times. Denote the results by n_1, n_2, \dots, n_P .

2. Output

$$\frac{1}{P} \sum_{p=1}^P \frac{\mathbf{x}(n_p)\mathbf{y}(n_p)}{h_{n_p}}$$

as an approximation of the inner product.

By simple analysis, it can be confirmed that the mean and variance of the above output are (\mathbf{x}, \mathbf{y}) and $\{\|\mathbf{x}\|^2\|\mathbf{y}\|^2 - (\mathbf{x}, \mathbf{y})^2\}/P$. The error of the approximation is independent of the dimensionality of the vectors. When we use the binary search tree data structure explained in the Algorithm section for the input vectors, we can perform this randomized algorithm in $O(\log N)$ time.

Acknowledgements

The authors would like to thank Chikako Koide for preparing the environment for the analysis.

Conflict of interest

The authors declare no competing financial interests.

Author contributions

NK and KM designed the study. NK and KM developed algorithms. NK performed analysis. NK and KM wrote the manuscript.

References

1. Hotelling H (1936) Relations Between Two Sets of Variates. *Biometrika* 28(3/4):321–377.
2. Smith SM, et al. (2015) A positive-negative mode of population covariation links brain connectivity, demographics and behavior. *Nature Neuroscience* 18(11):1565–1567.
3. Cowen AS, Keltner D (2017) Self-report captures 27 distinct categories of emotion bridged by continuous gradients. *Proceedings of the National Academy of Sciences* 114(38):E7900–E7909.
4. Fujiwara Y, Miyawaki Y, Kamitani Y (2013) Modular Encoding and Decoding Models Derived from Bayesian Canonical Correlation Analysis. *Neural Computation* 25(4):979–1005.
5. Nakanishi M, Wang Y, Wang Y-T, Jung T-P (2015) A Comparison Study of Canonical Correlation Analysis Based Methods for Detecting Steady-State Visual Evoked Potentials. *PLOS ONE* 10(10):e0140703.
6. Yamanishi Y, Vert J-P, Kanehisa M (2004) Protein network inference from multiple genomic data: a supervised approach. *Bioinformatics* 20(Suppl 1):i363–i370.
7. Waaijenborg S, Verselewe de Witt Hamer PC, Zwinderman AH (2008) Quantifying the Association between Gene Expressions and DNA-Markers by Penalized Canonical Correlation Analysis. *Statistical Applications in Genetics and Molecular Biology* 7(1). doi:10.2202/1544-6115.1329.
8. Witten DM, Tibshirani R, Hastie T (2009) A penalized matrix decomposition, with applications to sparse principal components and canonical correlation analysis. *Biostatistics* 10(3):515–534.
9. González I, et al. (2009) Highlighting relationships between heterogeneous biological data Through graphical displays based on regularized canonical correlation analysis. *Journal of Biological Systems* 17(02):173–199.
10. Cao L, Ju Z, Li J, Jian R, Jiang C (2015) Sequence detection analysis based on canonical correlation for steady-state visual evoked potential brain computer interfaces. *J Neurosci Methods* 253:10–17.
11. Fang J, et al. (2016) Joint sparse canonical correlation analysis for detecting differential imaging genetics modules. *Bioinformatics*:btw485.
12. Rousu J, Agranoff DD, Sodeinde O, Shawe-Taylor J, Fernandez-Reyes D (2013) Biomarker Discovery by Sparse Canonical Correlation Analysis of Complex Clinical Phenotypes of Tuberculosis and Malaria. *PLoS Computational Biology* 9(4):e1003018.
13. Seoane JA, Campbell C, Day INM, Casas JP, Gaunt TR (2014) Canonical Correlation Analysis for Gene-Based Pleiotropy Discovery. *PLoS Computational Biology* 10(10):e1003876.

14. Baur B, Bozdogan S (2015) A canonical correlation analysis-based dynamic bayesian network prior to infer gene regulatory networks from multiple types of biological data. *J Comput Biol* 22(4):289–299.
15. Sarkar BK, Chakraborty C (2015) DNA pattern recognition using canonical correlation algorithm. *J Biosci* 40(4):709–719.
16. Cichonska A, et al. (2016) metaCCA: summary statistics-based multivariate meta-analysis of genome-wide association studies using canonical correlation analysis. *Bioinformatics* 32(13):1981–1989.
17. Tang E (2019) A quantum-inspired classical algorithm for recommendation systems. *Proceedings of the 51st Annual ACM SIGACT Symposium on Theory of Computing - STOC 2019*:217–228.
18. Tang E (2018) Quantum-inspired classical algorithms for principal component analysis and supervised clustering. *arXiv:181100414 [quant-ph]*. Available at: <http://arxiv.org/abs/1811.00414> [Accessed June 23, 2019].
19. Gilyén A, Lloyd S, Tang E (2018) Quantum-inspired low-rank stochastic regression with logarithmic dependence on the dimension. *arXiv:181104909 [quant-ph]*. Available at: <http://arxiv.org/abs/1811.04909> [Accessed June 23, 2019].
20. Chia N-H, Lin H-H, Wang C (2018) Quantum-inspired sublinear classical algorithms for solving low-rank linear systems. *arXiv:181104852 [quant-ph]*. Available at: <http://arxiv.org/abs/1811.04852> [Accessed June 23, 2019].
21. Chia N-H, Li T, Lin H-H, Wang C (2019) Quantum-inspired classical sublinear-time algorithm for solving low-rank semidefinite programming via sampling approaches. *arXiv:190103254 [quant-ph]*. Available at: <http://arxiv.org/abs/1901.03254> [Accessed June 23, 2019].
22. Lai PL, Fyfe C (2000) Kernel and nonlinear canonical correlation analysis. *Int J Neural Syst* 10(5):365–377.
23. Akaho S (2001) A kernel method for canonical correlation analysis. In *Proceedings of the International Meeting of the Psychometric Society (IMPS2001)* (Springer-Verlag).
24. Melzer T, Reiter M, Bischof H (2001) Nonlinear Feature Extraction Using Generalized Canonical Correlation Analysis. *Artificial Neural Networks — ICANN 2001*, eds Dorffner G, Bischof H, Hornik K (Springer Berlin Heidelberg), pp 353–360.
25. Van Gestel T, Suykens JAK, De Brabanter J, De Moor B, Vandewalle J (2001) Kernel Canonical Correlation Analysis and Least Squares Support Vector Machines. *Artificial Neural Networks — ICANN 2001*, eds Dorffner G, Bischof H, Hornik K (Springer Berlin Heidelberg), pp 384–389.
26. Bach FR, Jordan MI (2002) Kernel Independent Component Analysis. *Journal of Machine Learning Research* 3:1–48.
27. Galen Andrew, Raman Arora, Jeff Bilmes, Karen Livescu (2013) Deep Canonical

- Correlation Analysis. *Proceedings of the 30th International Conference on Machine Learning*, eds Sanjoy Dasgupta, David McAllester (PMLR), pp 1247–1255.
28. Weiran Wang, Raman Arora, Karen Livescu, Jeff Bilmes (2015) On Deep Multi-View Representation Learning. *Proceedings of the 32nd International Conference on Machine Learning*, eds Francis Bach, David Blei (PMLR), pp 1083–1092.
 29. Frieze A, Kannan R, Vempala S (1998) Fast Monte-Carlo algorithms for finding low-rank approximations. *Proceedings 39th Annual Symposium on Foundations of Computer Science (Cat. No.98CB36280)*, pp 370–378.
 30. Harrow AW, Hassidim A, Lloyd S (2009) Quantum Algorithm for Linear Systems of Equations. *Physical Review Letters* 103(15). doi:10.1103/PhysRevLett.103.150502.
 31. Lloyd S, Mohseni M, Rebentrost P (2014) Quantum principal component analysis. *Nature Physics* 10(9):631–633.
 32. Rebentrost P, Mohseni M, Lloyd S (2014) Quantum Support Vector Machine for Big Data Classification. *Physical Review Letters* 113(13). doi:10.1103/PhysRevLett.113.130503.
 33. Biamonte J, et al. (2017) Quantum machine learning. *Nature* 549(7671):195–202.
 34. Kerenidis I, Prakash A (2016) Quantum Recommendation Systems. *arXiv:160308675 [quant-ph]*. Available at: <http://arxiv.org/abs/1603.08675> [Accessed June 25, 2019].
 35. Bach FR, Jordan MI (2005) A probabilistic interpretation of canonical correlation analysis. *Technical Report 688, Department of Statistics, University of California, Berkeley*.
 36. Lecun Y, Bottou L, Bengio Y, Haffner P (1998) Gradient-based learning applied to document recognition. *Proceedings of the IEEE* 86(11):2278–2324.